frontiers | Frontiers in Mechanical Engineering

TYPE Original Research
PUBLISHED 09 July 2024
DOI 10.3389/fmech.2024.1422412

OPEN ACCESS

EDITED BY
Qiang Li,
Technical University of Berlin, Germany

REVIEWED BY
Milan Bukvic,
University of Kragujevac, Serbia
Saša Milojević,
University of Kragujevac Faculty of Engineering, Serbia

*CORRESPONDENCE
Hikaru Okubo,
okubo-hikaru-xp@ynu.ac.jp

RECEIVED 24 April 2024
ACCEPTED 14 June 2024
PUBLISHED 09 July 2024

CITATION
Okubo H, Ishikawa T, Hashiba H, Inamochi T and Nakano K (2024), *In-situ* vibrational spectroscopic observation for thermally activated structural changes of 100% cellulose nanofiber molding with ultralow friction. *Front. Mech. Eng* 10:1422412. doi: 10.3389/fmech.2024.1422412

In-situ vibrational spectroscopic observation for thermally activated structural changes of 100% cellulose nanofiber molding with ultralow friction

Hikaru Okubo[1]*, Tomori Ishikawa[1], Hiromi Hashiba[2], Toru Inamochi[2] and Ken Nakano[1]

[1]Faculty of Environment and Information Sciences, Yokohama National University, Yokohama, Japan, [2]Chuetsu Pulp & Paper Co Ltd., Takaoka, Japan

This paper reports the thermally activated ultralow friction of 100% cellulose nanofiber (CNF) molding. The mechanism of friction reduction was investigated using a laboratory-built *in-situ* Raman tribometer. Our experimental results showed that a CNF molding exhibited an ultralow friction coefficient of below 0.04 in a CNF ring and steel disk tribopair under high-temperature conditions ($T >$ 100°C). The results of the temperature-rise friction test showed that the friction coefficient of the CNF molding strongly depended on the temperature and decreased linearly with increasing temperature. The *in situ* tribo-Raman monitoring results, during friction, indicated a change in the structure of the CNF molding. Therefore, the crystallinity indices and lengths of the CNF fibers gradually changed as the temperature increased. Moreover, transfer tribofilms were observed on the counter-steel surface against the CNF rings. When the CNF molding exhibited thermally activated ultralow friction, the tribofilm was mainly composed of cellulose and graphitic carbon. Our results suggest that the thermal and friction-activated structural transformations of CNF molding and CNF-derived transfer film formation are pivotal factors contributing to the ultralow friction phenomenon observed in CNF molding at high temperatures.

KEYWORDS

cellulose nanofibers, CNF, ultralow friction, Raman, *in-situ*, transfer film

1 Introduction

Cellulose nanofibers (CNFs) have recently been studied and developed as next-generation industrial biomass material (Posada et al., 2020). CNF is a biomass material with a fiber-like structure composed of cellulose microfibrils, which are aggregates of cellulose molecules. These molecules are five times stronger than steel and has a low specific density of 1/5. Owing to these excellent properties, CNFs are increasingly used as substitutes for petroleum-derived materials in industries. Especially, CNF offers a wide range of applications in many fields, including sensor technology, cosmetics, catalysis, energy production, water remediation, near-paper industry, petroleum industry and applications, and medicine (Zhang et al., 2019; Sanad et al., 2023) A novel use of CNF is a "100% CNF molding" (hereafter referred to as "CNF molding"), which is composed entirely of CNF. CNF molding is a biomass molding material

characterized by high strength, light weight, high thermal conductivity, and high processability. It is fabricated by pressurizing and dehydrating CNF dispersion liquids (Chuetsu Pulp and Paper Co, 2021). Although CNF moldings have strengths comparable to those of typical mechanical materials, such as steel and plastics, few studies have been conducted on the application of a CNF molding to fabricate mechanical elements, especially sliding mechanical elements that are expected to be used under severe operating conditions. However, the green transformation of sliding mechanical elements can be accelerated if CNF moldings are used to fabricate them.

A previous study reported the tribological properties of a CNF molding under various sliding conditions (Okubo et al., 2023a; Okubo et al., 2023b). In particular, the authors showed that a CNF molding exhibited a superlow friction coefficient of less than 0.01 when lubricated with a fatty-acid-containing oil, owing to the formation of a specific CNF swollen layer (Okubo et al., 2023b). Hence, controlling the structural transformation of a CNF molding at the frictional interface plays an important role in achieving ultralow friction in the molding. CNF moldings exhibit considerable potential as a ultralow-friction biomass material for various industrial applications. Numerous studies regarding low-friction materials, such as diamond-like carbon (DLC) and other carbon-related materials, have shown that conventional low-friction phenomena are often triggered by "thermal factors" (Enke, 1981; Zeng et al., 2015; Okubo et al., 2017; Zhu et al., 2021). In DLCs, sp^3 bonds transition to the more energetically stable sp^2 bonds with increasing thermal energy (Enke, 1981). In particular, under high-temperature conditions, DLC films at frictional interfaces undergo rapid structural evolutions owing to the complex interaction of the thermal, mechanical, and chemical effects due to friction. This results in ultralow friction owing to the formation of sp^2-rich tribofilms (Enke, 1981; Zeng et al., 2015; Agustin,et al., 2016; Okubo et al., 2017; Zhu et al., 2021). Several researchers have reported the thermal responses of CNFs under static conditions (non-friction) (Rubentheren et al., 2016; Okubo et al., 2019; Yang et al., 2019; Gan et al., 2020; Niskanen et al., 2022), and it is well known that high-temperature conditions cause changes in the crystalline structure of cellulose and in the breakdown of its networked structure. In our previous study, we confirmed that the amortization of a CNF molding was accelerated at tribological contacts under high-temperature conditions (Okubo et al., 2023a). However, the effects of temperature on the tribological properties of CNF molds are unclear.

The time-resolved observation of frictional surfaces is a promising method for understanding the lubrication mechanisms of tribological materials (Okubo and Sasaki, 2017; Okubo et al., 2020a; Okubo et al., 2020b). In our previous studies, we conducted "*in-situ* tribo-Raman spectroscopic measurements," which can be used to monitor the tribochemical reactions at the frictional interfaces during friction processes, to reveal the lubrication mechanisms of tribological materials (Okubo and Sasaki, 2017; Okubo et al., 2020a; Okubo et al., 2020b). The *in situ* tribo-Raman method can be used to effectively reveal the lubrication mechanisms of a material because the time-resolved Raman signals derived from the frictional interface can provide the degree of structural and compositional changes in materials during operation. Therefore, the operando tribo-Raman method has the potential to reveal the lubrication mechanism of CNF moldings.

In this study, the effect of test temperature on the tribological properties of a CNF molding was investigated. Tribological tests were performed using a ring-on-disk tribometer for a CNF ring and steel disk tribo-pairs under dry sliding conditions. To elucidate the effect of temperature on the tribological properties of the CNF molding, temperature rise and fall tests were conducted using a lab-built *in-situ* Raman tribometer (Okubo and Sasaki, 2017; Okubo et al., 2020a; Okubo et al., 2020b) that monitors frictional behavior. Additionally, time-resolved Raman spectra were obtained from the CNF ring under friction. Our results suggest that the thermal and friction-activated structural transformations of CNF molding and CNF-derived transfer film formation are pivotal factors contributing to the ultralow friction phenomenon. Moreover, our results accelerate the social implementation of the CNF molding as 100% biomass tribological materials for the sliding components.

2 Materials and methods

2.1 Materials

AISI52100 bearing steel (HV750, S_a:0.05 μm) was used for the steel disk (20 mm square) specimen. A CNF molding (nanoforest-CMB, JP, density = 1.41 g/cm^3, S_a = 0.05–0.1 μm, nanoindentation hardness = 0.37 GPa, XRD crystallinity = 80%, molecular weight *M*w = 133,000) was made from CNF water dispersions, which were prepared via the aqueous counter collision method (nanoforest, Chuetsu Pulp and Paper Co, 2021). The molding was used as a ring specimen (φ 20 mm × t 5 mm). The procedure for preparing the CNF molding has been described in previous studies (Okubo et al., 2023a; Okubo et al., 2023b).

2.2 Test apparatus and test procedures

A ring-on-disk friction tester equipped with a Raman spectroscope (Raman Touch YNU, Nanophoton Co., JP) was used for the friction tests, as shown in Figure 1A. To investigate the effects of the test temperature on the frictional properties and structure of the CNF molding, two friction tests were conducted: a constant-temperature friction test and a temperature-rise *in-situ* Raman friction test. The constant-temperature friction test was conducted under the following experimental conditions: load = 10 N, temperature: 30°C and 100°C, Hertz maximum contact pressure ≈0.15 GPa, relative humidity = 50–70%, sliding speed = 10 mm/s, and sliding time = 30 min. For the temperature-rise friction test, the friction test and Raman imaging analysis were performed alternately and intermittently at each of the following temperatures: 30, 50, 60, 70, 80, 90, 100, 110, and 120°C, as shown in Figure 1B. The friction test conditions (S1–S9 in Figure 1B) were as follows: load = 10 N, Hertz maximum contact pressure ≈0.15 GPa, relative humidity = 50–70%, sliding speed = 10 mm/s, and sliding time = 60 s at each temperature. Raman imaging (R0–R9 in Figure 1B) was performed on the CNF ring using a laser line scanning system (wavenumber: 532 nm, glid: 600 g/mm, exposure time: 1.0 s, and accumulated time: 1). Each image of

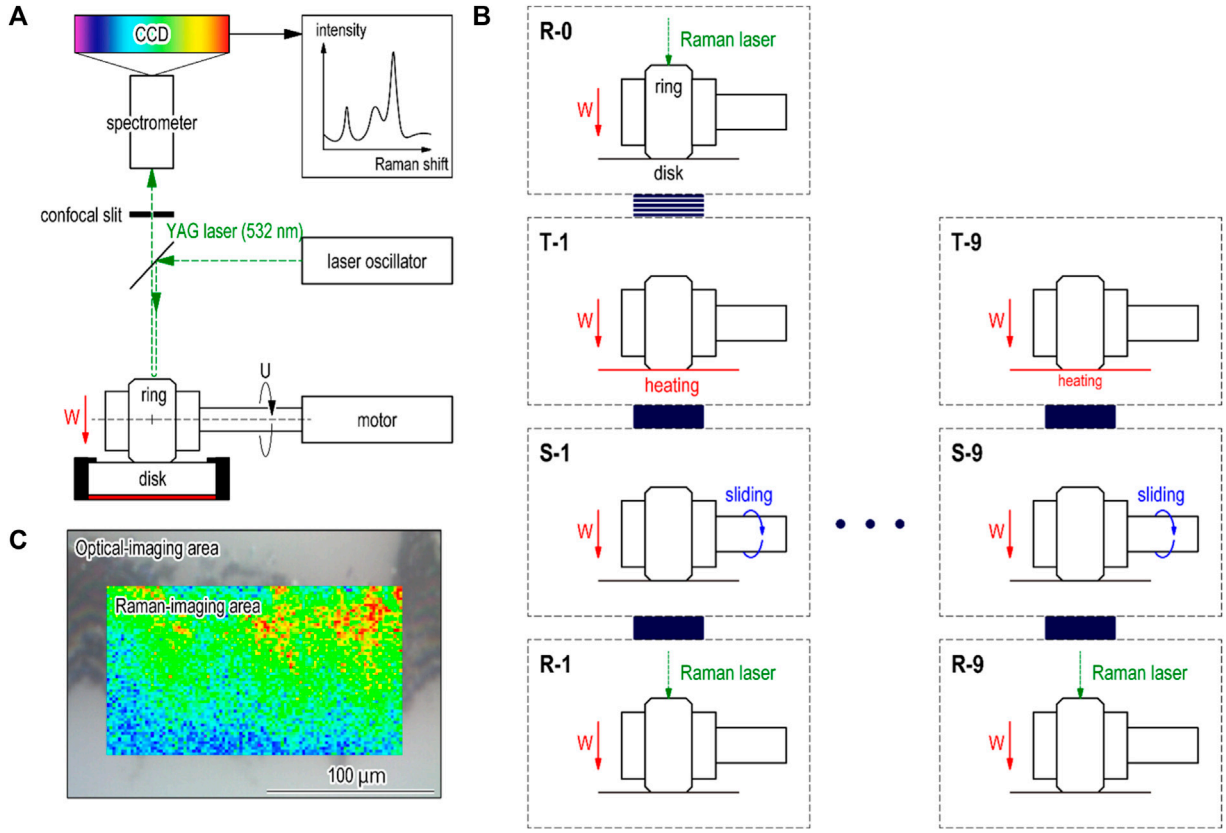

FIGURE 1
(A) Schematic of the developed apparatus for *in situ* Raman spectroscopy for observing frictional processes, **(B)** procedure of the temperature-rise friction test, and **(C)** a representative Raman-imaging result.

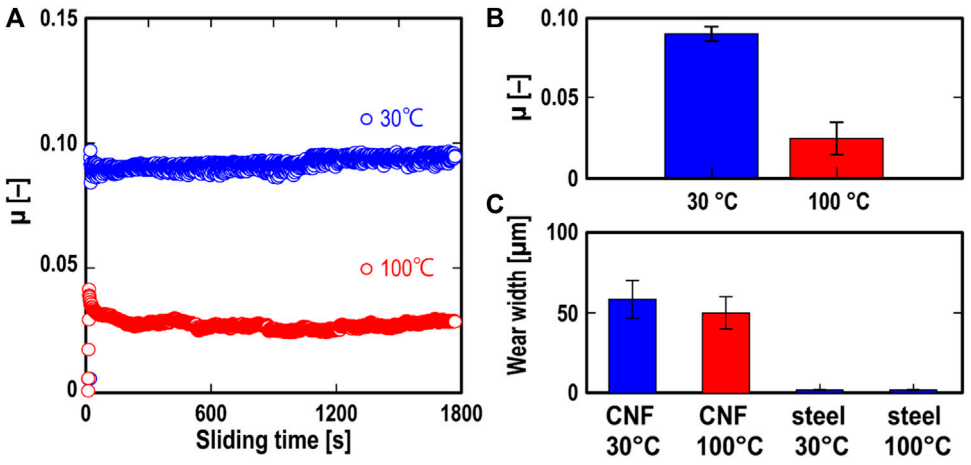

FIGURE 2
(A) Frictional behavior of the CNF/steel tribopair at test temperatures of 30°C and 100°C, **(B)** the average friction coefficient over 600 s calculated for each type of frictional behavior shown in Figure 1A, **(C)** the wear width of the CNF molding and steel surface.

the Raman spectrum consists of 5,000–6,000 pixels, with the pixel dimensions of height × width = 1.9 μm × 1.6 μm, as shown in Figure 1C. Atomic force microscopy (AFM) measurements (MultiMode8, Bruker Co., United States) were conducted on the worn steel surfaces to characterize the tribofilm using a pyramidal cantilever (PPP-NCHR AFM Probe, Nanosensor Co., CHE).

In this study, all friction tests and surface analyses were conducted more than three times to confirm the repeatability.

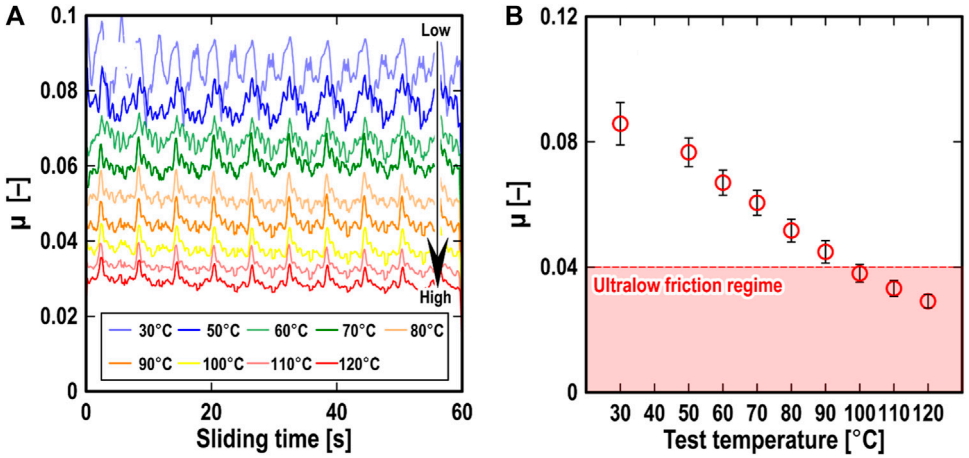

FIGURE 3
(A) Frictional behavior of the CNF/steel tribopair at test temperatures of 25°C and 100°C, **(B)** average friction coefficient over 600 s calculated for each type of frictional behavior shown in Figures 1A, C the wear width of the CNF molding and steel surface.

3 Results

3.1 Constant temperature friction test

Figure 2 shows the friction and wear properties of the CNF ring and steel disk tribopair at the temperatures of 30°C and 100°C. As shown in Figures 2A, B, the frictional properties of the CNF molding considerably differ between the temperatures of 30°C and 100°C. At 30°C, the friction coefficient exhibits an almost stable value of 0.095 during the tests. The friction coefficient is also stable at 100°C but has a value of 0.035 during the test, which is in the ultralow friction regime (below 0.04).

Figure 2C shows the wear widths of the CNF ring and steel disk under each condition. No significant difference is observed between the wear properties of each specimen (CNF ring and steel disk) at the temperatures of 30°C and 100°C, although the frictional performance strongly depended on the temperatures, as mentioned above. In the subsequent sections, we focus only on the friction properties of CNF molding because the wear performance is independent of the test temperature.

3.2 Temperature-rise friction test

Figures 3A, B show the frictional behavior and average friction coefficient of the CNF ring and steel disk tribopair, respectively, at each temperature in the temperature-rise friction test (the procedure is shown in Figure 1B). As shown in Figures 3A, B, the friction coefficient of the CNF ring and steel disk tribopair strongly depends on the test temperature, decreasing gradually from 0.09 to 0.025 as the temperature increases from 30°C to 120°C. The results of the temperature-rise friction test show that the frictional performance of CNF molding strongly depends on the test temperature, and thermal effects play a crucial role in achieving ultralow-friction performance of CNF molding.

3.3 *In situ* Raman monitoring

Figure 4 shows the representative *in situ* Raman spectra of the as-molded and worn surfaces of the CNF molding at each temperature. As shown in Figure 4A, the shifts in the Raman spectrum from 200 to 1,200 cm^{-1} indicate the presence of CNF-derived peaks. The peaks observed at 380, 430–450, 510, 891, 990, 1,057, and 1,090 cm^{-1} are assigned to CCC, CCO, and CO ring deformations, CCC and CCO ring deformations, COC glycosidic link deformation, vibration of the cellulose lateral unit at the crystal regions, CH_2 deformation, CO_2 alcohol stretching, and COC glycosidic link deformation, respectively (Li and Renneckar, 2011). Moreover, as shown in Figure 4B, the peaks observed at 2,890 and 3,200 cm^{-1} are assigned to the CH and CH_2 stretching vibrations and the OH stretching vibrations of water and cellulose, respectively (Li and Renneckar, 2011; Rossetti et al., 2023). Cellulose is a crystalline polymer, and its higher-order structure consists of a crystalline component with a regular arrangement and an amorphous component with a disordered structure. Raman analysis can be used to evaluate the factors related to the crystalline regions of cellulose using several methods (Agarwal et al., 2010). Following previous studies, the Raman-peak-height intensity ratios I_{370}/I_{1057} and I_{3200}/I_{2892} were used as indices of the crystallinity of the CNF-molded surfaces. Moreover, the peak intensities at 510 cm^{-1} and 890 cm^{-1} correspond to the lengths of the COC glycosidic chains (Li and Renneckar, 2011). Hence, the Raman-peak-height intensity ratios I_{510}/I_{1057} and I_{891}/I_{1057} were used as indices for the length of the COC glycosidic chains on the CNF molding surfaces.

Figure 5 shows the optical images and Raman imaging results of all indices obtained from the worn surface of the CNF molding for each temperature in the temperature-rise friction test. Figure 6 shows the temperature-dependent behavior of the average value of all indices obtained from the intensity ratio of the Raman spectrum for each pixel in the Raman images. As shown in Figure 5, the higher the intensity ratio in the images, the higher the crystallinity or the longer the COC glycosidic chain length in the

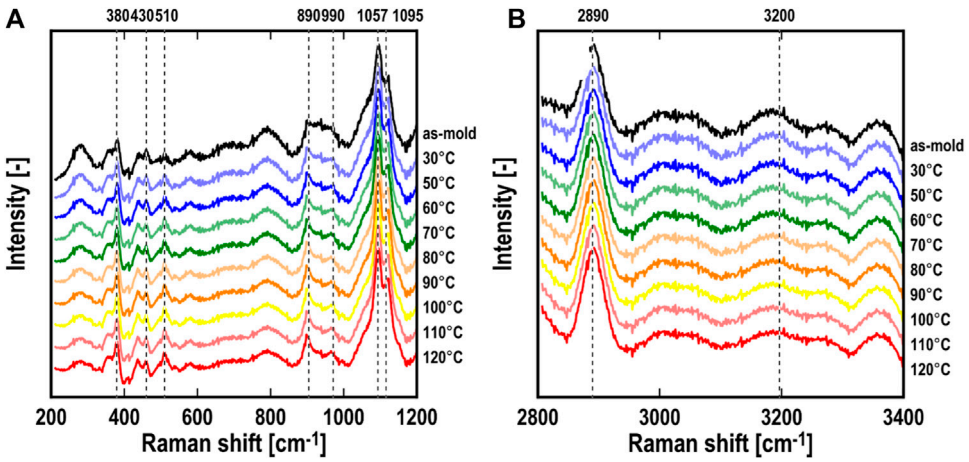

FIGURE 4
(A) *In situ* Raman spectra from 200 to 1,200 cm^{-1} for each temperature in the temperature-rise friction test, and **(B)** *in situ* Raman spectra from 2,800 to 3,400 cm^{-1} for each temperature in the temperature-rise friction test.

CNF molding, and *vice versa*. As shown in Figure 5, the values of all the indices in the image uniformly and gradually decrease with increasing test temperature, indicating that the crystallinity and COC glycosidic chain length in the CNF molding gradually decrease with increasing test temperature. Hence, thermally activated structural changes in CNF molding occur at frictional interfaces, and these changes occur easily at relatively high temperatures.

Figure 7 shows the optical images of the worn surfaces of the steel disk after the temperature-rise friction test and the Raman spectrum of the transfer region. As shown in Figure 7A, a transfer film is formed on the steel surface. Figure 7B shows the CNF-derived Raman peaks observed at 1,057 (similarly to the Raman spectra in Figure 4) and 1,430 cm^{-1}. These peaks are related to the CH deformation of the CNF (Li and Renneckar, 2011) and indicate that the tribofilm is a transfer film derived from the CNF molding. Two specific peaks, a D peak induced by disorder sp^2 carbon and a first-order graphite-induced G peak at 1,352 and 1,580 cm^{-1}, respectively, which are assigned to carbon crystals (Zeng et al., 2015; Okubo et al., 2017), are observed, although these peaks were not observed for the CNF molding surfaces. Details of the composition of the transfer film are discussed later.

3.4 AFM measurement

In the previous sections, the transfer film formation was observed on the steel surface. Therefore, AFM measurements were performed on the CNF-derived transfer films to evaluate their characteristics. Figure 8 shows the AFM topographical images and distance curves of the out-of-the-transfer and transfer-film regions. As shown in Figures 8A, B, the transfer film has a thickness of approximately 300 nm. Moreover, as shown in Figures 8C, D, the AFM force-distance curve derived from the transfer film region indicates that the approach and retraction curves are separated because of the positive and negative squeeze forces. However, such behavior is not observed outside the tribofilm region. Miklozic and Spikes also observed this phenomenon in tribofilms derived from zinc dialkyl dithiophosphate on steel surfaces. Additionally, from the squeeze behavior in the force-distance curve (Miklozic and Spikes, 2005), the tribofilms on the outermost layer were inferred to exist as a viscous film. According to a previous report, a CNF-derived transfer film exists as a viscous film on a frictional surface.

4 Discussion

In this study, the thermally activated ultralow friction phenomena of CNF molding were observed, as shown in Figures 2, 3. The thermally activated structural changes in the CNF molding and transfer-film formation were observed using the *in situ* Raman monitoring method, as shown in Figures 5–7. In this section, the mechanisms of thermally activated ultralow friction in CNF molding are discussed.

As shown in Figures 5, 6, the Raman peak height intensity ratios I_{370}/I_{1057}, I_{510}/I_{1057}, I_{890}/I_{1057}, and I_{3200}/I_{2892} gradually decrease with increasing test temperature, indicating the occurrence of amorphization and a decrease in the length of the COC glycosidic chains of the CNF molding at the frictional interface. These changes proceeded easily at higher temperatures. It is well known that the amortization of CNF, that is, their defibration, is caused by mechanical (Iwamoto et al., 2008; Liu et al., 2020), chemical (Azizi Samir et al., 2005; Bondeson et al., 2006), and thermal processes (Niskanen et al., 2022). Hence, the synergistic mechanical and thermal effects accelerated the amorphization of CNF molding at the frictional interfaces.

By contrast, a thick and viscous CNF-derived transfer film was observed on the steel surface, as shown in Figures 7, 8. For various tribological materials, transfer film formation is a key factor in reducing friction under dry sliding conditions because the transfer film acts as a sacrificial layer to disperse frictional energy at the frictional interface. The friction-reduction mechanisms of DLC coatings under dry sliding conditions have often been explained

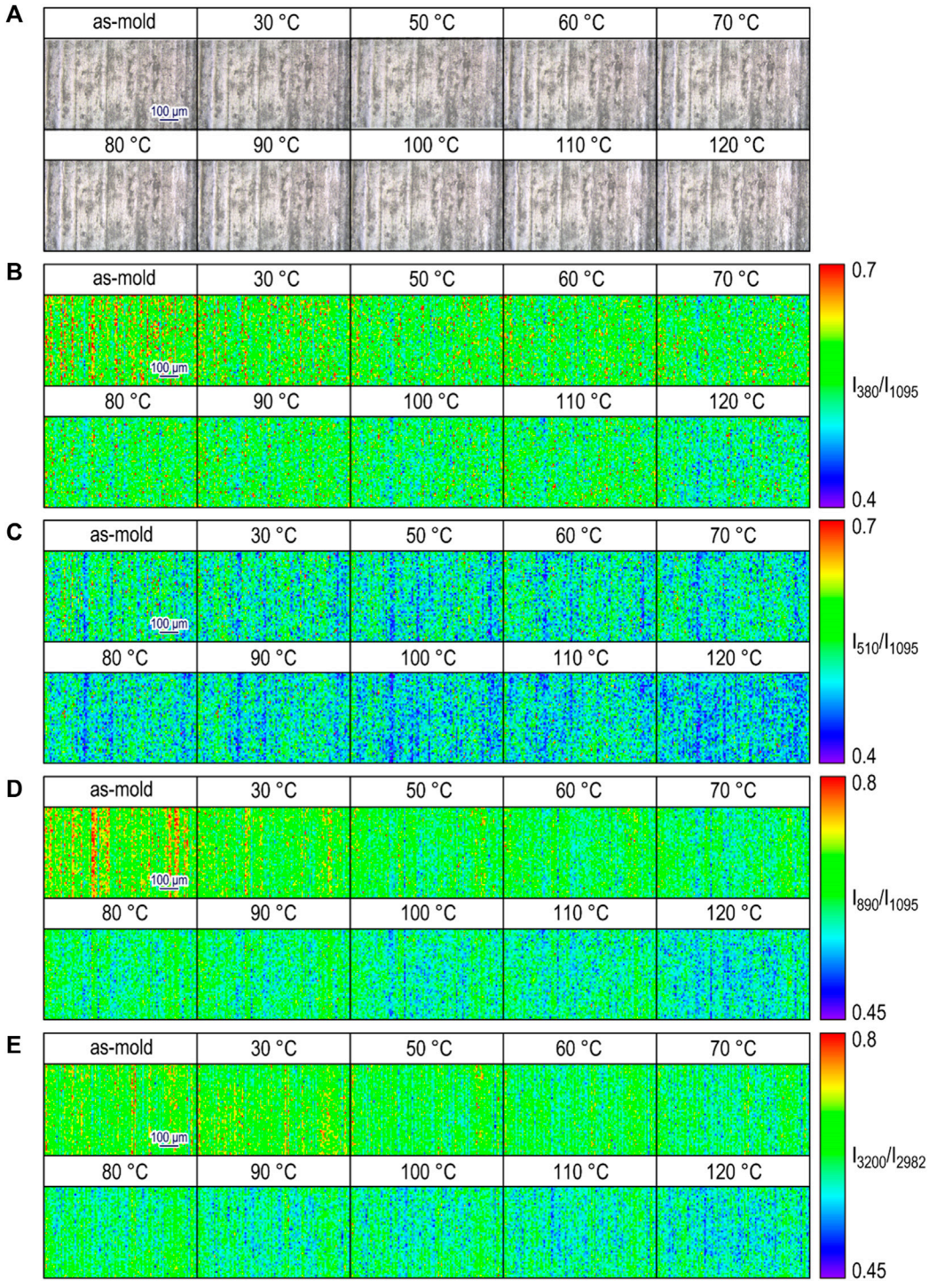

FIGURE 5
(A) Optical images of the as-molded and worn surfaces of the CNF molding, and *in situ* Raman-imaging results of **(B)** I_{380}/I_{1095}, **(C)** I_{510}/I_{1095}, **(D)** I_{890}/I_{1095}, and **(E)** I_{3200}/I_{1095} for each temperature in the temperature-rise friction test.

by the formation of a graphitization transfer layer on the counterface material against the DLC coating (Enke, 1981; Memming et al., 1986; Zeng et al., 2015; Okubo et al., 2017; Zhu et al., 2021). Memming et al. (1986) confirmed the formation of a carbon transfer film on the steel side when low friction was observed in the DLC/steel tribo-pair. This low friction was maintained by shifting from sliding between DLC and steel to sliding between DLC and the carbon transfer film. Erdemir et al. confirmed that such a carbon transfer layer was graphitized in the friction state and concluded that the continuous formation of the graphitization-transfer layer resulted in the low-friction behavior of the DLC coating (Erdemir et al., 1995). As shown in Figures 7B, D and G peaks are observed in the Raman

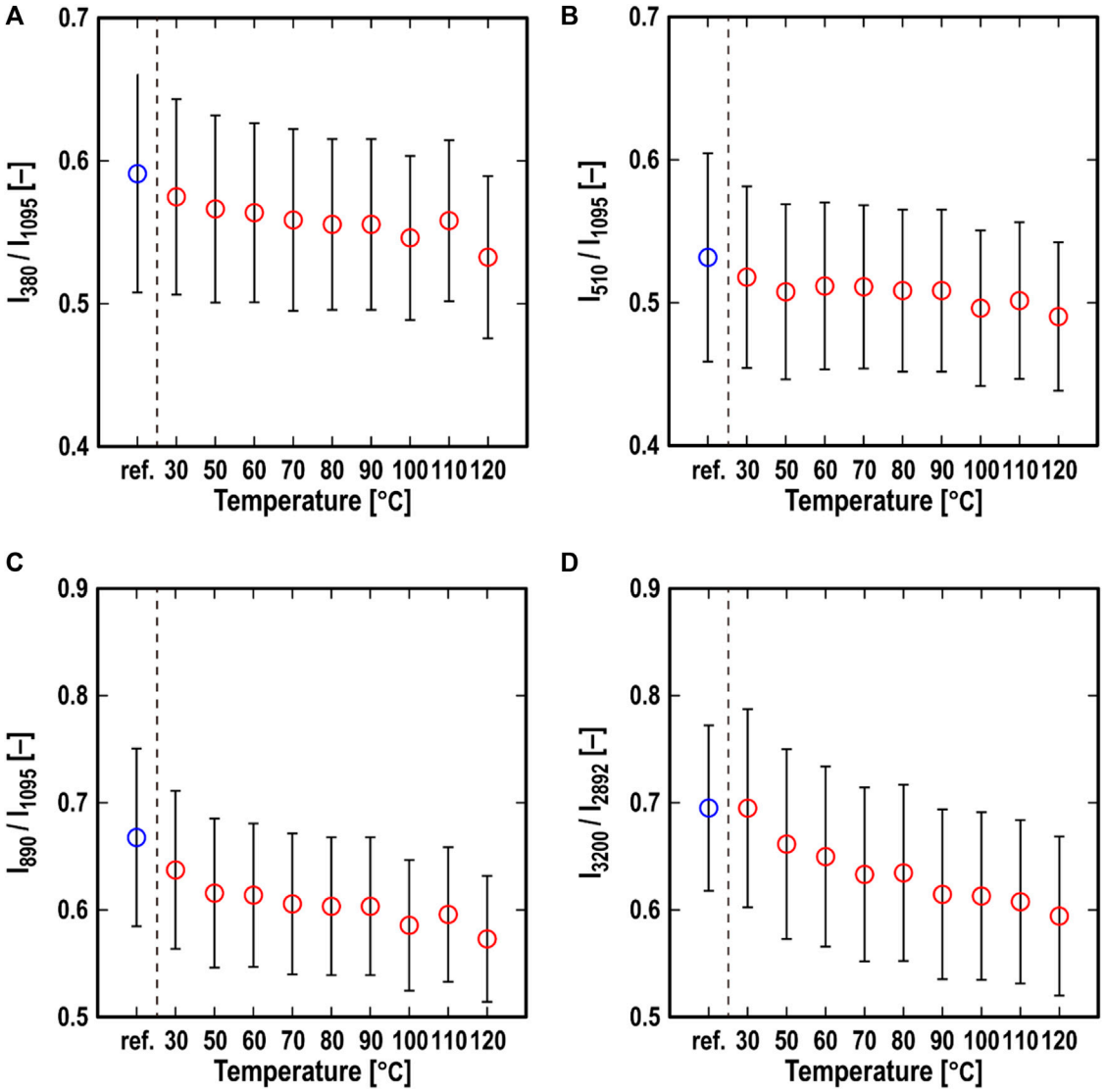

FIGURE 6
Temperature-dependent behavior of the averaged value of all indexes: **(A)** I_{380}/I_{1095}, **(B)** I_{510}/I_{1095}, **(C)** I_{890}/I_{1095}, and **(D)** I_{3200}/I_{1095} (the blue plot is the value for the as-molded surface) in the temperature-rise friction test.

spectra derived from the CNF-derived transfer layer, indicating that the CNF-derived transfer layer is also graphitized during the friction states in a manner similar to that of the DLC coatings (Zeng et al., 2015; Okubo et al., 2017). Figure 9 shows the Raman imaging of the I_{1352}/I_{1057} and I_{1580}/I_{1057} ratios of the relatively low frictional transfer film ($\mu < 0.03$) and high frictional transfer film ($\mu > 0.08$), which are defined by the amount of the sp^2 carbon in the CNF-derived transfer film. The low and high frictional transfer films were obtained after the friction test at a test temperature of 120°C and 30°C, respectively. As shown in Figures 9A, B, the two transfer films exhibit different values for both the ratios, although the formation of the transfer film is observed in both the low- and high-friction cases. Both ratios of the low-friction transfer film are higher in a large part of the film than those of the high-friction transfer film, indicating that the low-friction CNF-derived transfer film contains a larger amount of sp^2 carbon than the high-friction film.

Many researchers have reported that the graphitization of cellulose is induced by its thermal activation energy (Erdemir et al., 1995; Chen et al., 2018; Morosawa et al., 2021; Romero Millán et al., 2023). Morosawa et al. reported that strong thermal and optical effects occurred during the graphitization of CNF films when they were irradiated with femtosecond laser pulses (Rubentheren et al., 2016). Romero Millán et al. (2023) also reported that an iron-catalysis assistance and high-thermal energy (test temperature of 1,000°C–2000°C) promoted the graphitization of cellulose materials (Snad et al., 2023). Chen also reported that high-pressure (test pressure: 20 MPa) conditions and metal catalysis accelerated the graphitization of cellulose materials (Chen et al., 2018). Previous studies have suggested that cellulose materials can easily transform into graphitic carbon under high-temperature and high-pressure conditions. Furthermore, this transformation is accelerated in the presence of a metal catalyst. In this study, the maximum contact Hertzian pressure was approximately 50 MPa, which is much higher than the applied

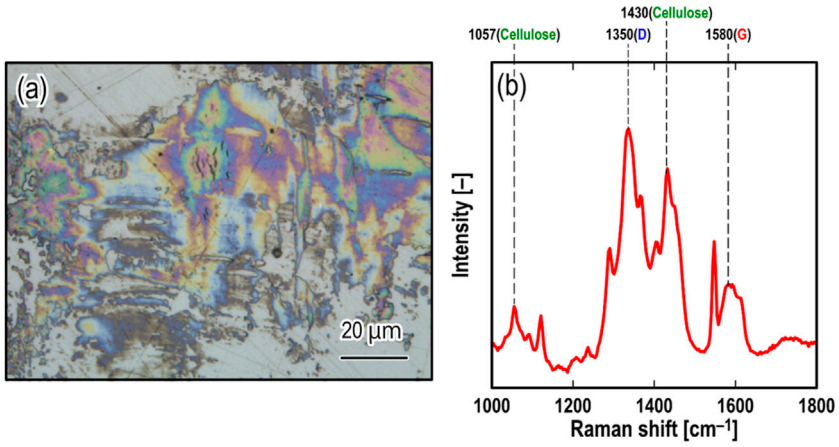

FIGURE 7
(A) Optical images of the worn surfaces of the steel disk after the temperature-rise friction test, and **(B)** the Raman spectrum of the transfer region.

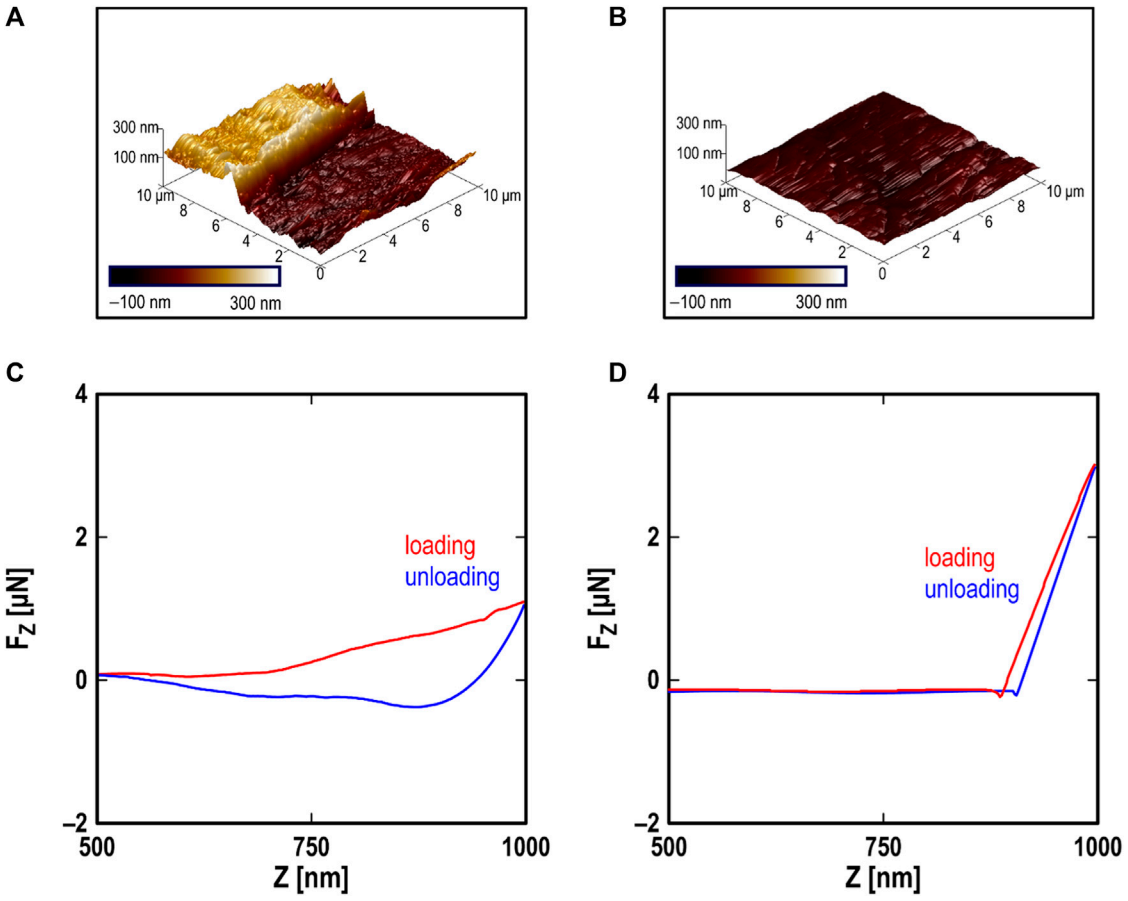

FIGURE 8
AFM topographical images of **(A)** the transfer film region and **(B)** the out-of-the-transfer film region, and AFM force-distance curves of the **(C)** transfer film region and **(D)** out-of-the-transfer film region.

pressure considered in most previous studies. The counter-faced material of the CNF molding, that is, the steel surface, might act as a catalyst. Moreover, the flash temperature, which is a friction-induced temperature increase, should be considered when discussing the thermal effects during friction. This is calculated using the following equation (Rabinowicz, 1965):

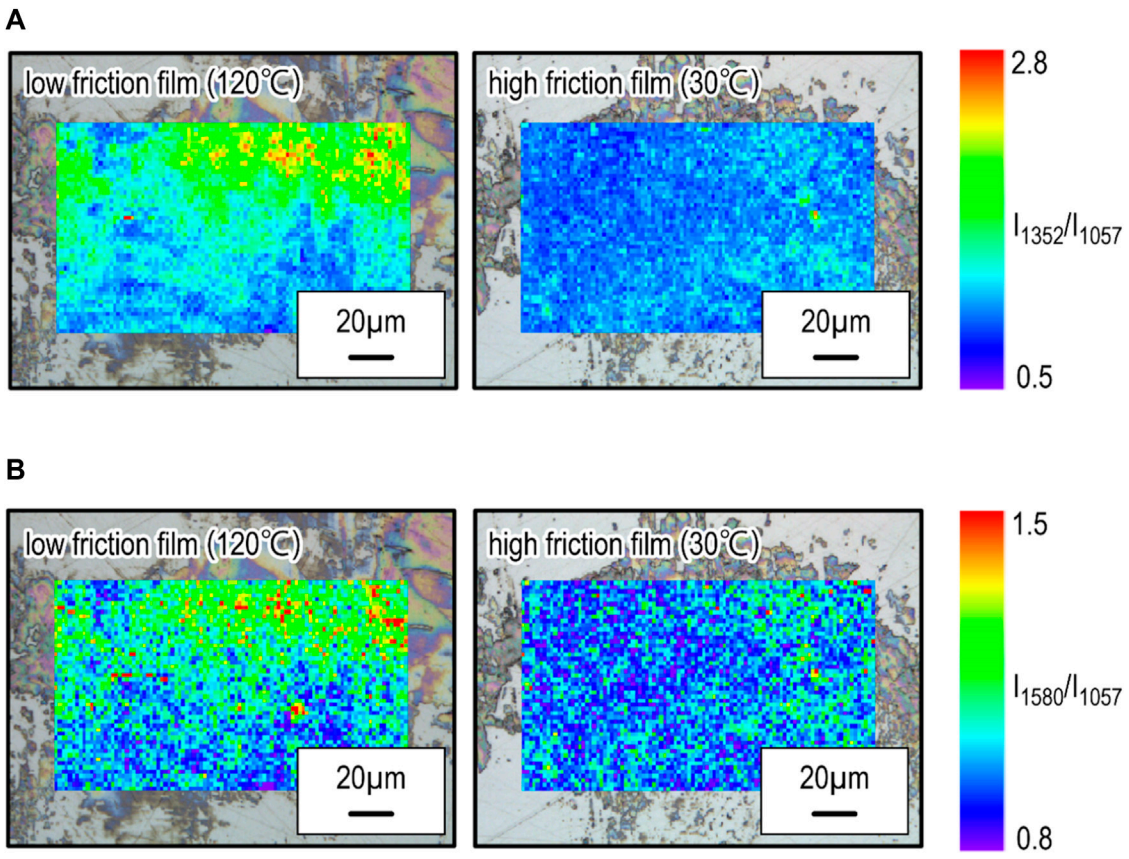

FIGURE 9
Raman images of **(A)** I_{1352}/I_{1057} and **(B)** I_{1580}/I_{1057} for the low friction (120°C) and high friction (30°C) transfer film on the steel surface.

$$\Delta T = \frac{\mu W V}{4Ja(k_1 + k_2)}$$

where ΔT is the change in the friction-induced temperature, μ is the friction coefficient, W is the applied load, V is the sliding speed, J is the heat equivalent, a is the contact radius, and $k_{1,2}$ is the thermal conductivity of each sliding material. At the asperity contacts of the CNF/steel tribo-pair surfaces, the above equation can be rewritten as follows.

$$\Delta T_{\mathrm{CNF/steel}} = \frac{\mu_{\mathrm{CNF/steel}} W V}{4Ja_{\mathrm{real}}(k_{\mathrm{CNF}} + k_{\mathrm{steel}})},$$

where $\Delta T_{\mathrm{CNF/steel}}$ is the change in the friction-induced temperature of the CNF/steel tribopair, $\mu_{\mathrm{CNF/steel}}$ is the friction coefficient of the CNF/steel tribopair, a_{real} is the real contact radius estimated from the AFM topographical image (Figure 8) and equals 10 nm, k_{CNF} is the thermal conductivity of the CNF molding and equals 2.0 W/(m/K), and k_{steel} is the thermal conductivity of the bearing steel [80 W/(m/K)]. According to rough parameter estimations, $\Delta T_{\mathrm{CNF/steel}}$ was approximately 300°C–900°C, depending on the friction coefficient and asperity size. Therefore, the thermal energy input into the sliding surface is sufficient to graphitize the CNF molding surface.

Based on the above results and estimations, Figure 10 shows a schematic of the mechanisms by which the thermally activated ultralow friction was generated in the CNF/steel tribopair. Frictional shear or thermal energy breaks the hydrogen and glycosidic bonds in cellulose molecular chains, resulting in the formation of glucose monomers or oligomers (Wang et al., 2021). This tendency is illustrated in Figures 5, 6. The formed glucose is then aromatized, and C=O groups are formed by the dehydration of the hydroxyl groups in the monomer (Wang et al., 2021). C=C bonds are formed via keto–enol tautomerism or intramolecular dehydration, whereas aromatic molecules are formed via intramolecular condensation or aldol reactions (Wang et al., 2021). Finally, microcrystalline graphite and aromatic clusters are formed at the frictional interfaces. Based on the above pathway, the graphitization of CNF molding proceeds at the frictional interface, and a low-frictional transfer film forms on the counter-face steel surface, resulting in ultralow friction of the CNF/steel tribopair at relatively high temperatures.

Generally, many researchers have reported that the graphitization of cellulose requires large amounts of thermal activation energy (Chen et al., 2018; Morosawa et al., 2021; Romero Millán et al., 2023). On the other hand, in this study, the test temperature that the graphitization of cellulose is observed is just 120°C although the set temperature to cause the graphitization of cellulose is above 1,000°C in the previous study. This indicates that the friction-assisted graphitization method proposed in this study, which is efficient and requires low energy, has the potential to be a novel method for efficiently producing graphitic carbon from biomass.

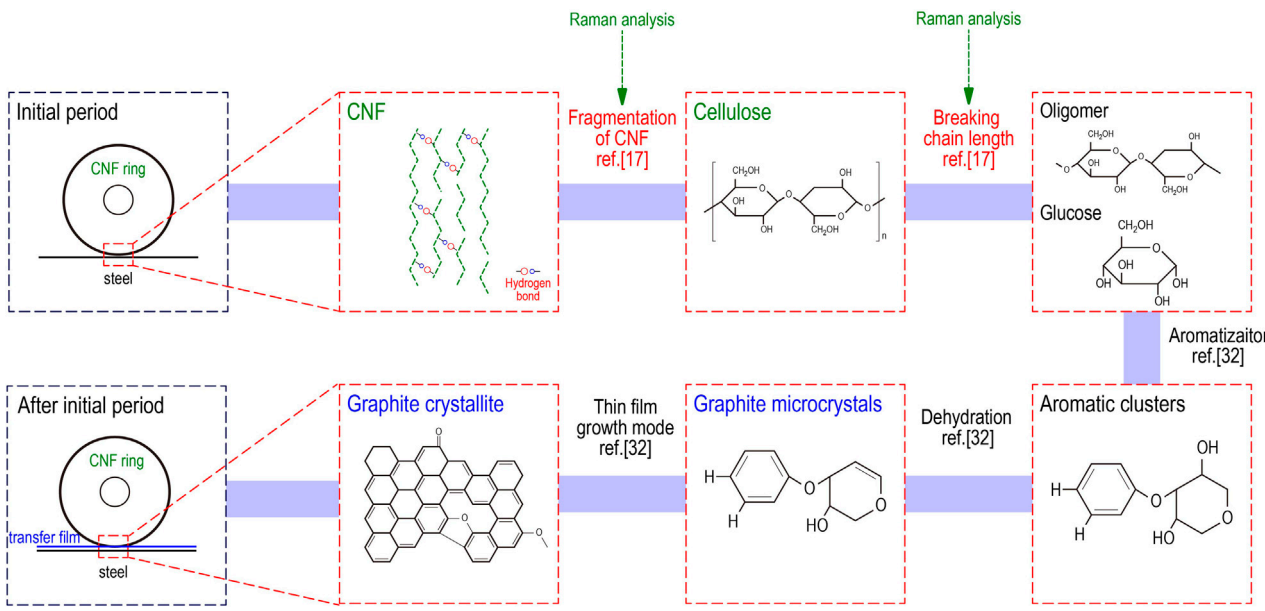

FIGURE 10
Schematic of the formation of ultralow frictional graphitized CNF-transfer film.

5 Conclusion

In this study, the effect of the test temperature on the tribological properties of CNF molding was investigated using *in situ* Raman monitoring for friction-induced CNF structural changes. In particular, the mechanisms of thermally activated ultralow friction in CNF molding were examined. The conclusions are as follows.

1. A CNF molding exhibits an ultralow friction coefficient below 0.04 at temperatures exceeding 100°C.
2. The crystallinity and the length of the COC glycosidic chain of a CNF molding gradually decreases at the frictional interfaces as the test temperature increases.
3. The formation of a graphitized CNF transfer film plays an important role in achieving ultralow friction in a CNF molding at high temperatures.

Data availability statement

The original contributions presented in the study are included in the article/Supplementary Material, further inquiries can be directed to the corresponding author.

Author contributions

HO: Conceptualization, Investigation, Visualization, Writing–original draft, Writing–review and editing. TI: Investigation, Writing–review and editing. HH: Investigation, Resources, Writing–review and editing. TI: Investigation, Resources, Writing–review and editing. KN: Supervision, Writing–original draft, Writing–review and editing.

Funding

The author(s) declare that financial support was received for the research, authorship, and/or publication of this article. This study was supported by ACT-X (JPMJAX23D4) from the Japan Science and Technology Agency (JST), and the Transmission Research Association for Mobility Innovation (22B2-01).

Conflict of interest

Authors HH and TI were employed by Chuetsu Pulp & Paper Co Ltd.

The remaining authors declare that the research was conducted in the absence of any commercial or financial relationships that could be construed as a potential conflict of interest.

Publisher's note

References

Agarwal, U. P., Reiner, R. S., and Ralph, S. A. (2010). Cellulose I crystallinity determination using FT-Raman spectroscopy: univariate and multivariate methods. *Cellulose* 17, 721–733. doi:10.1007/s10570-010-9420-z

Agustin, M. B., Nakatsubo, F., and Yano, H. (2016). The thermal stability of nanocellulose and its acetates with different degree of polymerization. *Cellulose* 23, 451–464. doi:10.1007/s10570-015-0813-x

Azizi Samir, M. A. S., Alloin, F., and Dufresne, A. (2005). Review of recent research into cellulosic whiskers, their properties and their application in nanocomposite field. *Biomacromol* 6, 612–626. doi:10.1021/bm0493685

Bondeson, D., Mathew, A., and Oksman, K. (2006). Optimization of the isolation of nanocrystals from microcrystalline cellulose by acid hydrolysis. *Cellulose* 13, 171–180. doi:10.1007/s10570-006-9061-4

Chen, C., Sun, K., Wang, A., Wang, S., and Jiang, J. (2018). Catalytic graphitization of cellulose using nickel as catalyst. *BioRes* 13 (2), 3165–3176. doi:10.15376/biores.13.2.3165-3176

Chuetsu Pulp and Paper Co. *Chuetsu Pulp and Paper Co, Nanoforest Ltd* (2021), Available at: https://www.chuetsu-pulp.co.jp/wordpress/wp-content/uploads/2021/05/nanoforest.pdf (Accessed June 16, 2022).

Enke, K. (1981). Some new results on the fabrication of and the mechanical, electrical, and optical properties of i-carbon layers. *Thin Solid Films* 80, 227–234. doi:10.1016/0040-6090(81)90226-1

Erdemir, A., Bindal, C., Pagan, J., and Wilbur, P. (1995). Characterization of transfer layers on steel surfaces sliding against diamond-like hydrocarbon films in dry nitrogen. *Surf. Coat. Technol.* 76–77, 559–563. doi:10.1016/02578-9729(50)25189-

Gan, P. G., Sam, S. T., Abdullah, M., and Omar, M. F. (2020). Thermal properties of nanocellulose-reinforced composites: a review. *J. Appl. Polym. Sci.* 137, 48544. doi:10.1002/app.48544

Iwamoto, S., Abe, K., and Yano, H. (2008). The effect of hemicelluloses on wood pulp nanofibrillation and nanofiber network characteristics. *Biomacromol* 9, 1022–1026. doi:10.1021/bm701157n

Li, Q., and Renneckar, S. (2011). Supramolecular structure characterization of molecularly thin cellulose I nanoparticles. *Biomacromol* 12, 650–659. doi:10.1021/bm101315y

Liu, Q., Chen, J., Yang, X., Qiao, C., Li, Z., Xu, C., et al. (2020). Synthesis, structure, and properties of N-2-hydroxylpropyl-3- trimethylammonium-O-carboxymethyl chitosan derivatives. *Int. J. Biol. Macromol.* 144, 568–577. doi:10.1016/j.ijbiomac.2019.12.125

Memming, R., Tolle, H. J., and Wierenga, P. E. (1986). Properties of polymeric layers of amorphous hydrogenated carbon produced by a plasma-activated chemical vapour deposition process I: spectroscopic investigations. *Thin Solid Films* 143 (3), 279–289. doi:10.1016/0040-6090(86)90181-1

Miklozic, K. T., and Spikes, H. A. (2005). Application of atomic force microscopy to the study of lubricant additive films. *J. Tribol.* 257, 405–415. doi:10.1115/1.1843159

Morosawa, F., Hayashi, S., and Terakawa, M. (2021). Femtosecond laser-induced graphitization of transparent cellulose nanofiber films. *ACS Sustain. Chem. Eng.* 9, 2955–2961. doi:10.1021/acssuschemeng.0c09153

Niskanen, I., Zhang, K., Karzarjeddi, M., Liimatainen, H., Shibata, S., Hagen, N., et al. (2022). Optical properties of cellulose nanofibre films at high temperatures. *J. Polym. Res.* 29, 187. doi:10.1007/s10965-022-03019-0

Okubo, H., Hashiba, H., Inamochi, T., Sato, K., Sasaki, S., Yamada, K., et al. (2023b). Novel environmentally superior tribomaterial with superlow friction: 100% cellulose nanofiber molding. *Tribol. Lett.* 71, 83. doi:10.1007/s11249-023-01754-z

Okubo, H., Nakae, R., Daisuke, I., Yamada, K., Yao, S., Nakano, K., et al. (2023a). Tribological properties of 100% cellulose nanofiber (CNF) molding under dry- and boundary lubrication-conditions at CNF/steel contacts. *Cellulose* 30, 6887–6905. doi:10.1007/s10570-023-05309-2

Okubo, H., and Sasaki, S. (2017). *In situ* Raman observation of structural transformation of diamond-like carbon films lubricated with MoDTC solution: mechanism of wear acceleration of DLC films lubricated with MoDTC solution. *Tribol. Int.* 113, 399–410. doi:10.1016/j.triboint.2016.10.009

Okubo, H., Sasaki, S., Lancon, D., Frederic, J., and Thiebaut, B. (2020b). Tribo-Raman-SLIM observation for diamond-like carbon lubricated with fully formulated oils with different wear levels at DLC/steel contacts. *Wear* 454–455, 203326. doi:10.1016/j.wear.2020.203326

Okubo, H., Tadokoro, C., Hirata, Y., and Sasaki, S. (2017). *In situ* Raman observation of the graphitization process of tetrahedral amorphous carbon diamond-like carbon under boundary lubrication in poly-alpha-olefin with an organic friction modifier. *Tribol. Online* 12, 229–237. doi:10.2474/trol.12.229

Okubo, H., Tadokoro, C., and Sasaki, S. (2020a). *In situ* Raman-SLIM monitoring for the formation processes of MoDTC and ZDDP Tribofilms AT steel/steel contacts under boundary lubrication. *Tribol. Online* 15, 105–116. doi:10.2474/trol.15.105

Okubo, H., Tadokoro, C., Sumi, T., Tanaka, N., and Sasaki, S. (2019). Wear acceleration mechanism of diamond-like carbon (DLC) films lubricated with MoDTC solution: roles of tribofilm formation and structural transformation in wear acceleration of DLC films lubricated with MoDTC solution. *Tribol. Int.* 133, 271–287. doi:10.1016/j.triboint.2018.12.029

Posada, P., Velásquez-Cock, J., Gómez-Hoyos, C., Serpa Guerra, A. M., Lyulin, S. V., Kenny, J. M., et al. (2020). Drying and redispersion of plant cellulose nanofibers for industrial applications: a review. *Cellulose* 27, 10649–10670. doi:10.1007/s10570-020-03348-7

Rabinowicz, E. (1965). *Friction and wear of materials*. Hoboken, NJ. HardcoverWiley & Sons Ltd

Romero Millán, L. M., Ghogia, A. M., White, C. E., and Nzihou, A. (2023). Iron nanoparticles to catalyze graphitization of cellulose for energy storage applications. *ACS Appl. Nano Mat.* 6, 3549–3559. doi:10.1021/acsanm.2c05312

Rossetti, A., Paciaroni, A., Rossi, B., Bottari, C., Comez, L., Corezzi, S., et al. (2023). TEMPO-oxidized cellulose nanofibril/polyvalent cations hydrogels: a multifaceted view of network interactions and inner structure. *Cellulose* 30, 2951–2967. doi:10.1007/s10570-023-05058-2

Rubentheren, V., Ward, T. A., Chee, C. Y., Nair, P., Salami, E., and Fearday, C. (2016). Effects of heat treatment on chitosan nanocomposite film reinforced with nanocrystalline cellulose and tannic acid. *Carbohydr. Polym.* 140, 202–208. doi:10.1016/j.carbpol.2015.12.068

Sanad, M. N., Farouz, M., and ElFaham, M. M. (2023). Recent advancement in nano cellulose as a biomass-based adsorbent for heavy metal ions removal: a review of a sustainable waste management approach. *Adv. Eng. Lett.* 2 (4), 120–142. doi:10.46793/adeletters.2023.2.4.1

Wang, D. C., Yu, H. Y., Qi, D., Wu, Y., Chen, L., and Li, Z. (2021). Confined chemical transitions for direct extraction of conductive cellulose nanofibers with graphitized carbon shell at low temperature and pressure. *J. Am. Chem. Soc.* 143, 11620–11630. doi:10.1021/jacs.1c04710

Yang, W., Gao, Y., Zuo, C., Deng, Y., and Dai, H. (2019). Thermally-induced cellulose nanofibril films with near-complete ultraviolet-blocking and improved water resistance. *Carbohydr. Polym.* 223, 115050. doi:10.1016/j.carbpol.2019.115050

Zeng, Q., Eryilmaz, O., and Ali Erdemir, A. (2015). Superlubricity of the DLC films-related friction system at elevated temperature. *RSC Adv.* 5, 93147–93154. doi:10.1039/C5RA16084G

Zhang, X., Li, H., Zhang, W., Huang, Z., Tsui, C. P., Lu, C., et al. (2019). In-situ growth of polypyrrole onto bamboo cellulose-derived compressible carbon aerogels for high performance supercapacitors. *Electrochimica Acta* 301, 55–62. doi:10.1016/j.electacta.2019.01.166

Zhu, L., Dong, J., and Zeng, Q. (2021). High temperature solid/liquid lubrication behaviours of DLC films. *Lubr. Sci.* 33, 229–245. doi:10.1002/ls.1540